Accepted Manuscript

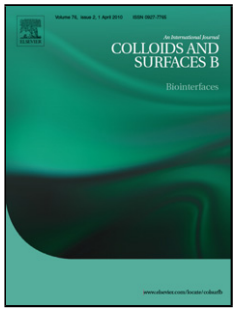

Title: Perspectives on Cavitation Enhanced Endothelial Layer Permeability

Authors: Giovanna Peruzzi, Giorgia Sinibaldi, Giulia Silvani, Giancarlo Ruocco, Carlo Massimo Casciola

PII: S0927-7765(18)30102-4
DOI: https://doi.org/10.1016/j.colsurfb.2018.02.027
Reference: COLSUB 9167

To appear in: *Colloids and Surfaces B: Biointerfaces*

Received date: 24-11-2017
Revised date: 6-2-2018
Accepted date: 11-2-2018

Please cite this article as: Giovanna Peruzzi, Giorgia Sinibaldi, Giulia Silvani, Giancarlo Ruocco, Carlo Massimo Casciola, Perspectives on Cavitation Enhanced Endothelial Layer Permeability, Colloids and Surfaces B: Biointerfaces https://doi.org/10.1016/j.colsurfb.2018.02.027

Perspectives on Cavitation Enhanced Endothelial Layer Permeability

Short statistical summary of the article:

Giovanna Peruzzi[1*], Giorgia Sinibaldi[2*], Giulia Silvani[1,2], Giancarlo Ruocco[1,3] and Carlo Massimo Casciola[1,2]

[1]Center for Life Nano Science@Sapienza, Istituto Italiano di Tecnologia, Rome, Italy.
[2]Department of Mechanical and Aerospace Engineering, Sapienza University of Rome, Italy.
[3]Department of Physics, Sapienza University of Rome, Italy.

*Authors contributed equally to the work

[*]**Corresponding Author**: giancarlo.ruocco@iit.it

Words: 6537
Figures: 8 + graphical abstract

Graphical Abstract

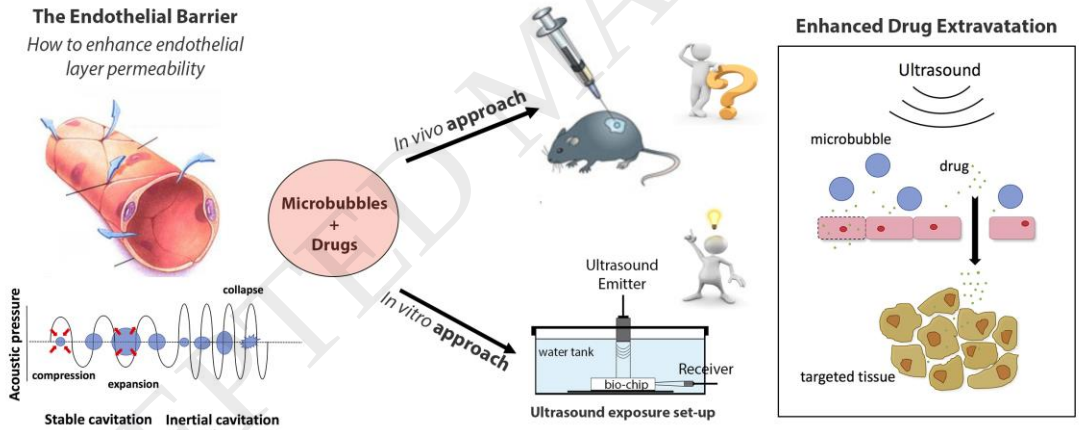

Highlights:

- Ultrasound irradiation of microbubbles may alter membrane permeability
- High-fidelity microvessels-on-chip allows to perform reliable *in vitro* studies on drug
- delivery
- Combining *in vitro* platforms and cavitation is crucial for improving targeted drug delivery

Abstract

Traditional drug delivery systems, where pharmaceutical agents are conveyed to the target tissue through the blood circulation, suffer of poor therapeutic efficiency and limited selectivity largely due to the low permeability of the highly specialised biological interface represented by the endothelial layer. Examples concern cancer therapeutics or degenerative disorders where drug delivery is inhibited by the blood-brain barrier (BBB). Micro-bubbles injected into the bloodstream undergo volume oscillations under localised ultrasound irradiation and possibly collapse near the site of interest, with no effect on the rest of the endothelium. The resulting mechanical action induces a transient increase of the inter-cellular spaces and facilitates drug extravasation. This approach, already pursed in *in vivo* animal models, is extremely expensive and time-consuming. On the other hand *in vitro* studies using different kinds of microfluidic networks are firmly established in the pharmaceutical industry for drug-delivery testing. The combination of the *in vitro* approach with ultrasound used to control micro-bubbles oscillations is expected to provide crucial information for developing cavitation enhanced drug delivery protocols and for screening the properties of the biological interface in presence of healthy or diseased tissues. Purpose of the present review is providing the state of the art in this rapidly growing field where cavitation is exploited as a viable technology to transiently modify the permeability of the biological interface. After describing current *in vivo* studies, particular emphasis will be placed on illustrating characteristics of micro-devices, biological functionalisation, properties of the artificial endothelium and ultrasound irradiation techniques.

Keywords: drug delivery systems, endothelial layer permeability, cavitation, ultrasound, micro-bubbles, microfluidics.

Table of Contents

1. Introduction

The outcome of drug administration may fail for insufficient drug accumulation at the desired site. The risk is prevented using larger doses than strictly needed, enhancing the complementary risk of body toxicity, a particularly crucial issue for potent anticancer drugs [1, 2]. In this context, targeted drug delivery concerns innovative technologies for the safe transport and release of pharmaceutical compounds to the specific site of action able to minimise systemic toxic side effects and improve therapeutic efficacy [3].

Controlled release dates back to the founder of chemotherapy, Paul Ehrlich who

inspired clinical treatment with “targeted success” [4] according to four rules: *retain*, *evade*, *target* and *release* [5], i.e. preserve the content till delivery; evade the immune system and target the site of release avoiding undesired effects.

Drugs administrated through the blood stream need to extravasate from blood vessels [6]. Extravasation is hampered by the endothelium that coats the vasculature , a layer of specialised cells around capillary vases tightened together to form a highly selective membrane that confines molecules larger than albumin to the circulation [7].

Current knowledge in cell biology can be combined with engineering to devise microfluidic systems aimed at developing innovative methods for endothelium permeability control [8]. Microfluidics, i.e. fluid manipulation at micrometrical scale [9], allows to reproduce the cellular microenvironment to study living systems under well controlled and reproducible conditions. It can be used, in particular, to check the endothelium response to different drug delivery protocols in healthy and diseased tissues.

Cavitation is especially promising for facilitating drug delivery given its ability to transiently and reversibly loosen the junctions sealing the endothelial cells together. Cavitation is obtained by combining ultrasound (US) exposure and microbubbles (MBs) injection. This technique, known as USMB-mediated drug delivery, is expected to develop into a potentially reliable and safe delivery method able to avoid irreversible damage to physiological barriers [10].

Microbubbles, already approved for human safety [11], were originally developed as contrast agents for ultrasound imaging [12-14] but are presently finding therapeutical application in drug delivery [11, 15-18]. Ultrasound contrast agents (UCA) comprise a shell and an encapsulated gas core and respond to US with different cavitation modes [19]. Stable cavitation upon low acoustic pressure induces acoustic microstreaming in the surrounding fluid environment. Inertial cavitation, obtained at higher acoustic pressure, is more violent with shock wave emission and intense micro-jet formation. The respective bioeffects on cells and tissues are different.

USMB-mediated approaches are especially important for transient opening and permeabilisation of the Blood-Brain Barrier (BBB) [15, 16, 20]. The BBB is a highly specialised structure of the central nervous system vasculature consisting of endothelial cells connected together by tight junctions, surrounded by perycites and packed by astrocytes [21]. It protects the brain from pathogens but, at the same time, blocks the entry of most pharmaceuticals [15].

The present review concerns cavitation assisted drug delivery with special focus on *in vitro* microdevices for delivery protocol development. Microfluidics and related microfabrication techniques are briefly described. After introducing the background on bubble dynamics and cavitation, a discussion of the biological effects of US induced MB dynamics is reported. Current *in vivo* applications in animal models are presented,

focusing on the BBB in particular. Finally, an overview of recent *in vitro* studies and their potential for drug delivery protocol development under controlled conditions is provided. Limits of present techniques and perspective development of more realistic biomimetic devices for a better reproduction of the microvascular environment are finally illustrated.

2. Microfluidics and drug delivery

With the development of microfluidics new approaches to study drug delivery become available paving the way to improved therapeutic efficiency. Microfluidic devices are exploited for developing drug carriers [22-25] able to enhance drug bioavailability and specificity, meanwhile reducing cytotoxicity. Microfluidic devices may be also exploited to improve drug delivery mechanisms [26, 27]. Relevant examples are the vasculature-on-a-chip to investigate *in vitro* disease models, including immunological research related to cell-to-cell interactions in tumours [28, 29], and the organs-on-chip to replicate organ functions [30, 31]. Within this new class of "bioinspired" devices, the present review is centred on devices able to reproduce physiological barriers in view of optimised drug uptake.

Microfluidic devices designed to mimic topologically complex networks are often realised in Polydimethylsiloxane (PDMS) [32, 33]. PDMS is an inexpensive polymer, flexible, optically transparent and easy to handle and bond to other surfaces. It is compatible with biological assays due to its permeability to gases, impermeability to water and nontoxicity to cells [34]. Despite many beneficial properties, there are limitations in the possible biomedical applications [30]. For example, PDMS may absorb small molecules which can affect cell signalling dynamics [35]. Its hydrophobicity prevents usage for capillarity-driven systems, e.g. in self-drive microdevices for Point-of-Care (POC) diagnostic and in electrophoresis. These inconveniences can be overcome by resorting to SU-8, an epoxy negative photoresist, inert to chemical reactions, impermeable and slightly hydrophilic with good adhesion on glass [36, 37].
The technology for fabricating microfluidic networks is soft lithography, based on rapid prototyping and replica moulding [32, 38]. The microfluidic network is conceived using Computer Aided Design (CAD) software and printed on a high-resolution mask to be used as photomask in contact photolithography. The dissolution of the unpolymerised photoresist produces a positive relief on a silicon wafer, that serves as moulding master. Once the master is available, a small series of microdevices can be cheaply obtained by replica moulding.

Focusing on platforms designed to reproduce the BBB, a prolific development took place in the last fifteen years. *In vitro* BBB models reproducing important features of the *in vivo* brain microenvironment have been developed in 2D and 3D microchips using cells co-cultured systems (e.g. in [39-43]). For a detailed review of the cell culture

models of brain endothelial cells see also [44], while a complete discussion of the related microfluidic aspects are discussed in [45].

The endothelial cell phenotype is established by shear stress (the frictional forces generated by the blood flow) exposure that induces functional cell responses to the environment through signalling molecules and/or cytoskeleton reorganisation [46-48]. Hence a crucial issue in mimicking vasculature systems is the reproduction of the mechanical stress acting on the endothelial barrier [49, 50].

The effect of flow conditions on vascular drug delivery can be addressed by *in vitro* flow chambers with idealised geometry, *e.g.* the parallel plate flow chambers, that simulates physiologic flows through perfusion at low Reynolds number [51]. Although this simple setting allows for an easy characterisation of flow-induced effects, the microcirculation is not reproduced, leading to poor correspondence with *in vivo* flow dynamics, cell and drug transport [52].
A more complete reconstruction of the microvascular environment is obtained in [53] with a disposable chip featuring flow and morphologically realistic environment that reproduces the leukocyte adhesion cascade.

The number of systems that include a physiologic flow component in BBB models is still limited [54-56]. A novel commercially available device has been recently developed as a model of BBB-on-a-chip [57, 58]. This device has been optimised with the main intent to investigate BBB permeability and for therapeutics screening. Main features of the BBB-on-a-chip are: visualisation and real-time measurement capability; channel three-dimensionality matching the size of vascular vessels; correct perfusion rate and physiological shear stress intensity; biochemical interactions between different cultured tissues. In particular, in [57] the neonatal stage BBB is reproduced *in vitro* by a co-culture of rat brain endothelial cells (RBEC) and astrocytes seeded in different compartments and kept in communication through a porous interface. The two distinct cell cultures communicating through a biointerface offer the opportunity to investigate the cell-cell interactions that occur between different tissues, e.g., immune system and tumour.

Experiments on the permeability of the artificially-grown endothelial layer in the BBB-on-a-chip were recently carried out in the authors laboratory. The BBB-on-a-chip is shown in the top panel of Fig.1 with a culture of human umbilical vein endothelial cells (HUVECs) in the vascular channels, obtained upon cells seeding and adhesion. The typical elongated shape, characteristic of endothelial cells under physiological blood flow rate, is obtained by exposing the cells to 22 hours flow [59]. The bottom panel of Fig.1 reports data concerning the endothelial membrane permeability evaluated by measuring fluorescent dye diffusion through the membrane pores. The protocol is typically based on 2-hour time lapse acquisitions under a confocal microscope operated in epifluorescence mode.

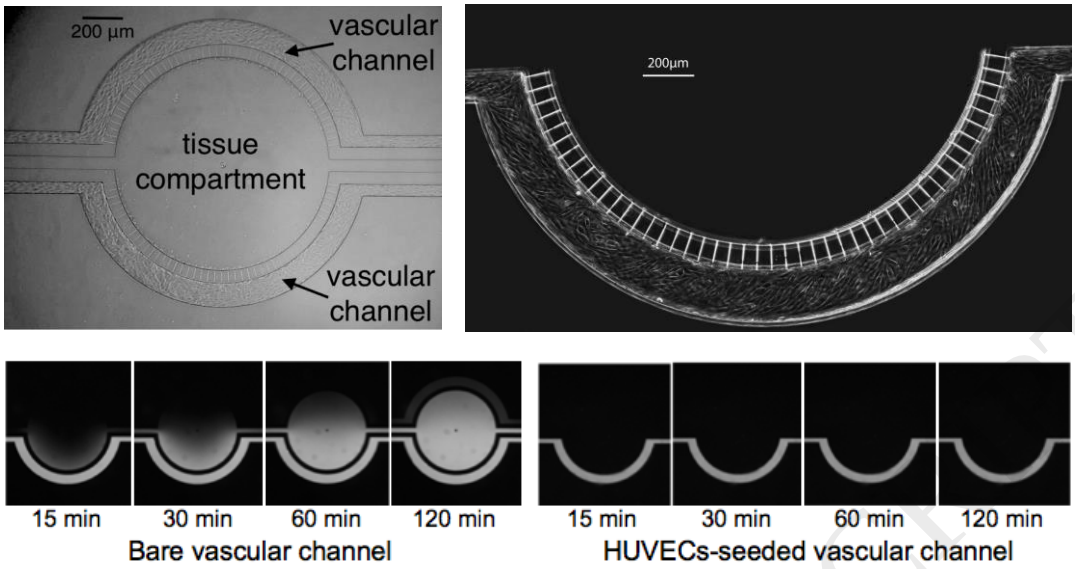

Figure 1. *(Top) Bright field images of the BBB-on-a-chip. On the left panel, the vascular channels seeded with HUVECs and the tissue compartment. On the right panel, reconstituted image of the vascular channel. HUVECs are visibly elongated following the flow direction resembling vessel endothelial cells. The interface consisting of a series of slits that allow communications between the compartments is clearly visible. (Bottom) Time lapse of the intensity change due to the accumulation of Texas Red 40 kDa dextran from the vascular channel to the tissue compartment. Vascular channel with no-cell seeding (bottom left) and with HUVECs coating (bottom right).*

Permeability is quantified through image analysis on the intensity change due to fluorescent accumulation in the tissue compartment [57]. The comparison between two different cases is presented: BBB-on-a-chip with bare vascular channels (bottom left) and seeded with confluent HUVECs (bottom right). In presence of endothelial cells, permeability decreases by two magnitude orders, thus indicating that the proper physiological response of the barrier is achieved.

3. Ultrasound cavitation

The physical basis of USMB-mediated drug delivery is the mechanical stress generated on the endothelium by bubble oscillations forced by US exposure. The oscillations induce a flow in the surrounding liquid that, through pressure and friction forces, facilitates drug release and increase drug uptake [11]. The main US parameters which characterise the phenomenon are:

1) Frequency, ranging from kHz to MHz, depending on specific tissue, type of MB and clinical purpose. Frequency influences the penetration depth and the spatial resolution

of US, with spatial resolutions increasing and penetration depth decreasing for larger frequency [60].

2) Intensity, for drug delivery applications between 0.3 - 3 W/cm^2 to limit the tissue temperature rise below 1°C.

3) Mechanical Index (MI), defined as the US peak negative pressure (PNP) divided by the square root of the frequency $p_{min}/\sqrt{f}$ [61]. The MI upper limit for clinical applications is set to 1.9 MPa/MHz, to prevent direct tissue damage [62]. An understanding of the role of these parameters requires a brief introduction to bubble dynamics, nucleation and inertial collapse.

The dynamics of a spherical bubble immersed in bulk liquid with constant density ρ_L and dynamic viscosity μ_L obeys the Rayleigh-Plesset equation [63],

$$\frac{p_B(t)-p_L^{\infty}(t)}{\rho_L} = R\ddot{R} + \frac{3}{2}\dot{R}^2 + \frac{4\mu_L}{\rho_L}\frac{\dot{R}}{R} + \frac{2\sigma}{\rho_L R},$$

for the time-dependent bubble radius $R(t)$. The equation is obtained by integrating the spherically symmetric Navier-Stokes system for a viscous liquid from the bubble radius to infinity. $p_B(t)$ is the pressure inside the bubble and σ the liquid/gas surface tension. The time dependent pressure $p_L^{\infty}(t)$ in the liquid due to the acoustic wave is the forcing term [64, 65]. The equation accounts for the Young-Laplace law relating pressure jump across the interface to surface tension and mean curvature $p_B - p_L^R = 2\sigma/R$, where p_L^R is the liquid pressure at the bubble interface. The inner pressure due to a mixture of gas and vapour is $p_B = p_V + p_G$, where p_G is the gas partial pressure and p_V the vapour pressure at the given conditions. $p_B(t)$ depends on time since the bubble oscillations compress and expand the gas and depends on the thermodynamic transformation undergone by the gas.

Bubble stability is assessed by considering the linearised form of the Rayleigh-Plesset equation for small radial perturbations. Given environment pressure and temperature, bubbles are stable (i.e. they return to equilibrium after perturbation removal) when they are smaller than a critical size (Blake radius, [66]) $R_c = \left[9M_g T K_g/(8\pi\gamma)\right]^{1/2}$ (M_g is the bubble mass, T the temperature and K_g the gas constant). The critical liquid pressure $p_L^c = p_V - 4\sigma/(3R_c)$ is the liquid pressure that expands the originally stable bubble to the critical radius [67, 68]). Hence, depending on acoustic amplitude, preexisting microbubbles, stable in the unperturbed conditions, may be destabilised by the acoustic pressure minimum. The unstable bubble may undergo inertial cavitation, i.e. expand up to a maximum radius and successively collapse. During this violent event, the gas compressed inside the bubble reaches very high temperatures. Moreover, when the collapse is arrested and the bubble re-expands back, a shock wave is emitted in the surrounding liquid [69-72]. MI combines the information on amplitude and frequency such that, below a threshold value (MI $\leq$ 1.9), the collapsing bubble does not damage neighbouring tissues by thermal and mechanical loads.

Tissue over-heating that may occur with continuous US application is prevented with discontinuous exposure, where pulses are repeated periodically (duty cycle), allowing time for energy dispersion. Concerning sources, US can be excited by non-focused (plane waves), or focused transducers. Plane waves are typically used in imaging, while focused transducers are suitable for therapy, where large energy density is needed in the target region while exposure of surrounding tissues is undesired. Reduction of energy deposition area can be achieved by focusing also with the relatively low frequencies needed to reach deep tissues [60].

A gas bubble containing a single gas with molecular weight m_w tends to dissolve in water as described by the Epstein-Plesset model [73],

$$\frac{dR}{dt} = -DHK_0T\frac{1-s+2\frac{m_w\gamma}{\rho K_0 TR}}{1+2\frac{m_w\gamma}{\rho K_0 TR}}\frac{1}{R},$$

where D is the gas diffusivity, H Henry's constant for the gas and K_0 the ideal gas constant. The dissolution rate depends on the gas saturation fraction of the liquid, $s = C/C_s$, ratio of dissolved gas to saturation concentration. Ordinary gas/water interfaces have a considerable surface tension, implying that, according to Young-Laplace law, the pressure inside micron sized bubbles may raise to large values (pressure increase of 1.4bar for 1μm radii). Since air is easily soluble in biological liquids, ordinary bubbles are fast to dissolve, unless properly stabilised. Stability increases (i.e. life time lengthens) for a larger saturation fraction, a smaller surface tension, $\sigma \to 0$, and smaller gas diffusivity and solubility. Since saturation level cannot be modified, bubble life time is enhanced by decreasing surface tension through suitable coatings and by reducing gas diffusivity and solubility using large molecular weight inert species. The coating shell also contributes to bubble longevity by reducing the interface permeability [74, 75]. Recently, coated bubbles, originally developed as ultrasound contrast agents (UCAs), acquired a key role as "ultrasound-triggered agents" for drug delivery and therapy [13, 14, 17, 76-78]. They consist of MBs (1 - 10 μm) of heavy molecular weight inert gas (e.g. SF_6, C_3F_8 or C_4F_{10}), coated with a lipid, polymer, sugar or protein layer.

Compared to uncoated air bubbles, UCAs have different mechanical properties, e.g. resonance frequency, viscous damping and scattering response [79-82]. At small acoustic pressures, they behave linearly, with symmetric expansion/compression cycles. At larger acoustic pressures (i.e., above 50 KPa), phospholipid-coated bubbles (e.g. SonoVue®) present a "compression-only" behaviour [83] due to the rigidity of the coating shell that can hardly expand. Large compressive stress during the positive pressure peak easily induces shell buckling and large compressive deformations. Large acoustic pressures eventually break the bubble shell and the bubble reverts to the classical Rayleigh-Plesset dynamics [82]. Several models are available (e.g. in [80-82,

84]) to account for the coating shell in the dynamics, see Fig. 2 for an illustration.

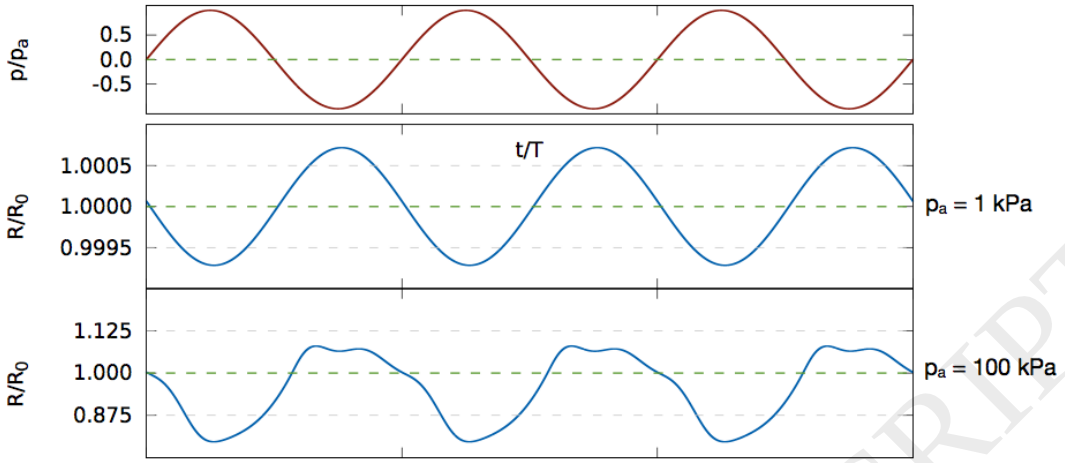

Figure 2. *Numerical solution of the Rayleigh-Plesset equation with the surface tension model reproducing the dynamics of a lipid-coated bubble [82]. Applied pressure wave (top row). Symmetric bubble response (middle row).“Compression-only” behaviour (bottom row). Courtesy of G. Di Muccio e M. Chinappi.*

The acoustic response described above is controlled by the MI [17, 18, 85]. At low MI (< 0.1, say) MBs oscillate linearly and scatter the acoustic signal at excitation frequency. Increasing the MI (0.1 - 0.3) stable cavitation persists in the non-linear regime, see Fig. 3, with large oscillations and super/sub-harmonic emission. In this regime bubbles significantly displace the surrounding liquid inducing acoustic microstreaming [86-88] which pattern depends on the bubble oscillation mode [89] and primarily varies with applied frequency, being most pronounced near the fundamental spherical mode.

Microstreaming plays a prominent role in USMB-mediated drug delivery and may be worth being discussed further. Beside volume oscillations, a bubble forced by an acoustic wave of amplitude a near the resonant (angular) frequency ω experiences a periodic (Bjerknes) force along the acoustic beam due to the front/aft pressure asymmetry,

$$F_B(t) = \oint_{\partial B} p\mathbf{n}dS \simeq \nabla p_L[\mathbf{x}_B(t), t]V_B(t),$$

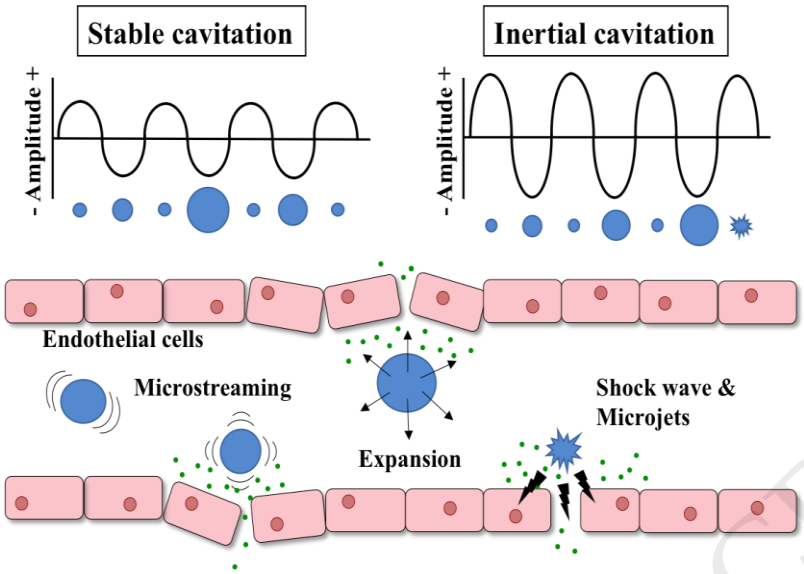

Figure 3. *Sketch of stable and inertial cavitation showing the effects on the endothelium.*

where $\mathbf{x}_B$ is the bubble centre and V_B its volume, and oscillates back and forth. The oscillating stream seen by the bubble produces an oscillating boundary layer of thickness $\delta = \sqrt{2\nu/\omega}$ [90]. Although the bubble centre moves proportionally to the amplitude a, the nonlinearity of the Navier-Stokes equations leads to a component of the boundary layer layer response proportional to the squared amplitude, $\mathbf{u}_{bl} = a\mathbf{u}_{bl}^{(1)}(\mathbf{x},t) + a^2[\mathbf{u}_{ss}(\mathbf{x}) + \mathbf{u}_{un}^{(2)}(\mathbf{x},t)]$. It consists of an oscillatory term and a time independent, steady streaming part, $\mathbf{u}_{ss}^{(2)}$. Its origin is the quadratic self-interaction of the first order term, $\mathbf{u}_{bl}^{(1)}$, proportional to $\cos(\omega t)$. Hence the quadratic self-interaction has non-vanishing time average coming from the squared cosine, $\cos(\omega t)^2 = 1/2[1 - \sin(2\omega t)]$. This produces the steady streaming response $\mathbf{u}_{ss}$ of the boundary layer which, in its turn, drives the liquid motion further away from the bubble. When volume oscillations are combined with the periodic displacement, the steady external velocity field turns out to be of dipole type [91] and decays slowly enough with distance from the bubble to significantly affect its surroundings. When the bubble is close to the endothelial layer, the shear stress due to the steady streaming produces loosen the cell junctions and facilitate drug extravasation [92].

The bubble response described so far concerns stable cavitation at moderate acoustic intensities. At higher acoustic pressure (0.3 < MI < 0.6) unstable bubble growth occurs which leads to inertial cavitation, accompanied by broadband acoustic emission. Also for the coated bubbles, inertial cavitation induces strong mechanical stresses on adjacent tissues, due to shock waves and high-speed liquid jets toward the endothelium.

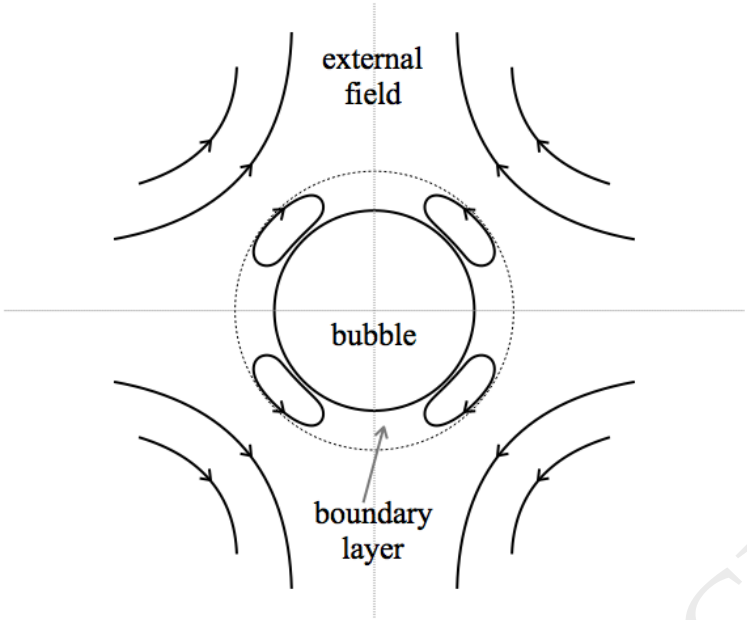

Figure 4. *Sketch of the steady streaming generated by a bubble under US exposure. The dotted line indicates the thickness of the unsteady boundary layer, inside which the steady streaming flow pattern in sketched by the closed streamlines. The steady streaming inside the boundary layer drives the external flow outside the boundary layer. In presence of combined volume and position oscillations of the bubble the external field has a dipolar structure which decays slowly with distance from the bubble.*

This may cause additional blood vessel permeabilisation and even cell membrane perforation [93].

A basic understanding of the phenomenology can be gained from Fig. 5 concerning a bubble collapse near a solid wall. The wall leads to an asymmetric collapse [94, 95] which deforms the originally spherical bubble into a toroid with a liquid jet perforating the bubble and impinging the wall. The collapse is arrested by the emission of the strong shock wave highlighted in the Fig 5d. The original literature on the topic, dating back to the 40's, dealt with bubbles generated by underwater explosions [96-98]. More recently the subject revived in the context of cavitation [99-101]. Since the mathematics is somewhat involved, only the relevant phenomenology is illustrated here.

The system comprising bubble and wall can be shown to be equivalent to two symmetric bubbles collapsing in free space, Fig. 5a. To a first approximation, the velocity corresponds to the potential flow of two symmetrically placed (negative) point sources (sinks), $\mathbf{u} = -A/4\pi((\mathbf{x}-\mathbf{x}_B)/|\mathbf{x}-\mathbf{x}_B|^3 + (\mathbf{x}-\mathbf{x}_I)/|\mathbf{x}-\mathbf{x}_I|^3)$, where the subscript I denotes the image bubble. The velocity on the bubble is sketched in Fig. 5b, where its distal side collapses faster than the proximal side. Consequently, the bubble flattens and its centre translates toward the wall. From the the bubble equation of motion,

$$M_e\ddot{z} = F_z = \oint p\vec{n}_z dS,$$

where M_e is the so-called bubble added mass (i.e. the effective mass of the displaced fluid [102]), this motion must be due to the pressure asymmetry between distal side and proximal side pushing the bubble toward the wall. Turning the argument around, this pressure difference is the mechanical cause of bubble motion and deformation. The successive stages are sketched in Fig. 5c, see e.g. [103]. A critical configuration is

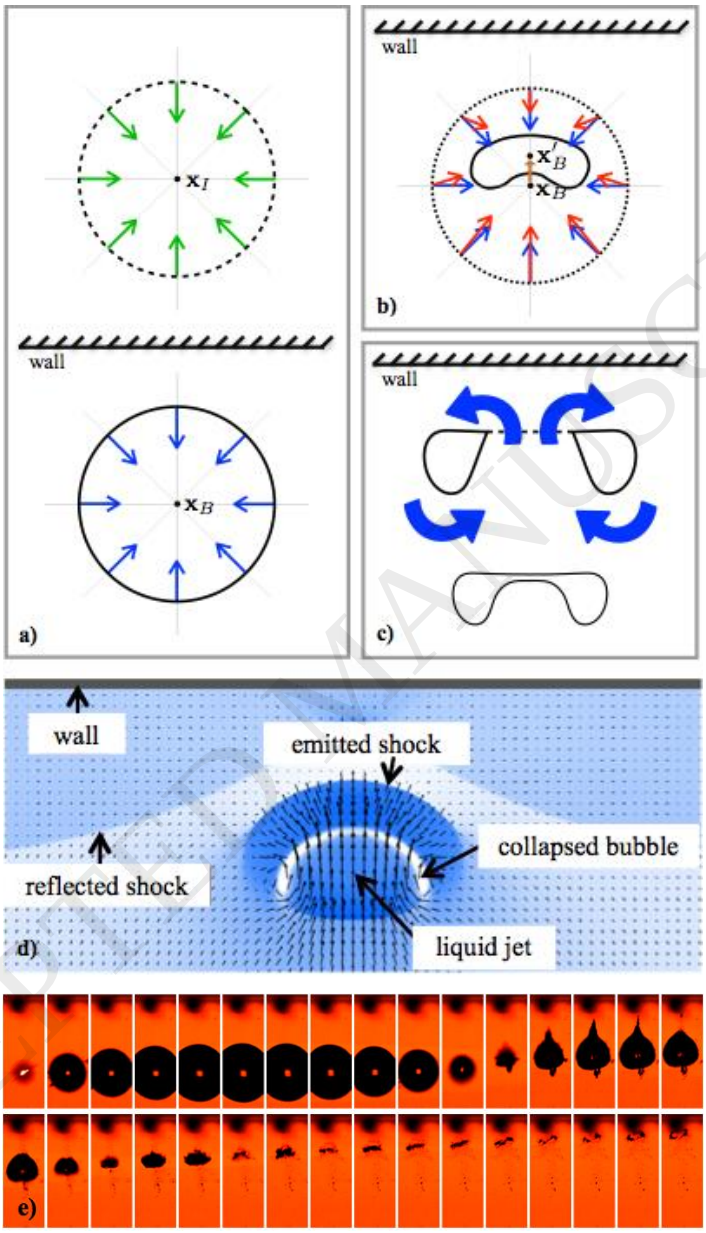

Figure 5. *Sketch of different phases of bubble collapse close to a boundary. a) collapsing bubble with centre x_B and its image with centre x_I; b) bubble deformation: the distal bubble side collapses faster than the proximal side; c) section of the toroidal-like bubble approaching the wall; d) numerical simulation of bubble collapse [94]: velocity field (arrows) and density field (contours); e) bubble dynamics in proximity of a solid surface, acquired at 40000 fps (frame numbered from left to right and top to bottom).*

reached when the distal part of the interface catches up with the proximal side. Finally capillary effects modify the bubble topology as sketched in Fig. 5c and the bubble develops into a toroidal shape. The flow domain outside the bubble becomes multiply connected allowing for a net circulation concatenated with the torus corresponding to the liquid jet accelerating toward the wall.

The results of recent numerical simulations with an advanced phase field model [104] carried out by some of the present authors to model bubble dynamics in extreme condition [105] are illustrated in Fig. 5d. All the phases of the process discussed above are reproduced by the simulations. The model accounts for the compressibility of both the vapour and the liquid phase and captures the emission of the strong shock wave, see also [72], as well as the topological change of the bubble shape leading to the successive jetting phase. This complex dynamics can be experimentally investigated in well controlled condition by focusing a pulsed laser in water. In Fig. 5e a sequence of images acquired in the dedicated set-up developed in the present author's lab shows the dynamics of a bubble nucleated in proximity of a surface. Here, the acquisition is obtained in background illumination with a fast camera at 40000 fps (frame per seconds). The setup consists of a Nd:YAG pulsed laser (532 nm wavelength, maximum pulse energy of 30 mJ, pulse duration of 8 ns) and an optical chain (beam expander and parabolic mirror) to expand, collimate and finally focus the laser beam in a box full of pure water. The characteristic phases of the bubble dynamics and its lifetime are strictly dependent on the amount of focused energy and the distance from the surface. For the specific conditions adopted in Fig. 5e, prior to the first collapse (frames 1-11), the bubble shape is not yet influenced by the surface. It approaches the wall until with successive rebounds the characteristic topology shown in Fig. 5b and 5c emerges (see the torus at frame n°32).

Cavitation can be monitored by so-called passive cavitation detection (PCD), an acoustic method to acquire bubble response exposed to US. An acoustic transducer is typically applied to passively listen for sound scattered by cavitation events. Mainly this method consists in a time-domain acquisition and frequency-domain analysis, after a combination of proper filtering to isolate the contribution of different cavitation phenomena. In general, stable cavitation results in emission at subharmonics and ultraharmonics of the main excitation frequency, while inertial cavitation reveals broadband noise emission above the characteristic background noise level [106]. Quantifying both broadband noise and subharmonics/ultraharmonics emission allows to estimate the so-called cavitation dose, which provides information about the intensity of cavitation events [107].

4. Ultrasound and microbubble-induced bioeffects

Molecule/compound passage through the endothelial barrier is tightly regulated and occurs through two specific transport pathways. In the transcellular pathway

(transcytosis) cell entry involves vesicles for molecule transport while in the paracellular pathway passage occurs between adjacent endothelial cells [108]. Endothelial cells are connected by cellular junctions that coordinately open and close to allow or deny passage. Specialised endothelial barriers involve different junctions, the most important ones for barrier selectivity being tight and adherens junctions. Tight junctions, found in the BBB, are mainly constituted of transmembrane adhesion proteins (occludins and claudins), Zonula Occludens proteins (ZO-1, 2 and 3) and JAM family proteins [109]. The typical protein in adherens junctions is the vascular endothelial cadherin (VE-cadherin), responsible for regulating vessel permeability [110, 111]. VE-cadherin is tightly connected to β-catenin and their association strengthens cell-cell adhesion forces [112]. Endothelial layer integrity modifications consequence of low intensity US exposure on HUVEC cells, say, can then be appreciated by β-catenin immunofluorescence staining able to visualise junction disruptions [113].

Beside loosening cells junctions, the mechanical stress induced by USMB application impacts on the endothelium by altering cell membrane integrity. Before discussing this issue, it is worth recalling that, apart from MBs, US alone may already induce transient cell membrane permeabilisation enhancing compound/molecule up-take through sonoporation [114-116]. In particular, low-intensity US application is known to induce on HUVECs bioeffects similar to USMB irradiation [113]. With MBs, the response is typically amplified.

The mechanical stress acting on the cellular membrane may result in pore formation and/or membrane invagination leading to endocytosis [117-119]. The former is a membrane disruption process through appearance of pore-like structures upon US-irradiation that increase membrane permeability [120, 121]. Endocytosis is instead an active transport-process mediated by membrane invaginations. Independent of pore formation, it is controlled by several molecules and organelles that guide specific endocytic pathways [122, 123]. Endocytosis contributes to USMB mediated delivery [124] by allowing uptake of macromolecules that cannot be accommodated through pores.

Molecule size dictates the endocytic mechanism upon USMB irradiation, as identified by the localisation of different sized conjugated dextran molecules inside, e.g., in primary endothelial cells *in vitro* or in rat femoral artery endothelium *in vivo* [124]. After USMB, small dextran molecules (range 4.4 - 70 kDa) are homogeneously distributed in the cytoplasm, implying uptake through membrane pores. Above a certain size (155 - 500 kDa) dextran localises instead inside endocytic compartments. The uptake route significantly depends on the applied acoustic pressure. Differential entry upon loading with different sized dextran-conjugated molecules (4 kDa-2 MDa) and different acoustic settings (PNP 100-500 kPa) was demonstrated in [119] using human melanoma (BLM) cells. Cells were isolated in two populations with low and high dextran content, respectively, using Fluorescence Activated Cell Sorting based on

dextran signal intensity. Notably, the acoustic pressure correlates with the dextran fluorescence signal and with different cellular uptake mechanism. The low intensity population presented punctate dots typical of endocytic compartments (endocytic uptake) whereas cytoplasmic diffuse distribution of the high intensity population indicated entry by pores [119]. At higher US intensity (500 kPa, inertial cavitation) transient pores appear on the membrane while low acoustic pressure (100 kPa, stable cavitation) produces cell membrane rearrangement leading to endocytosis.

In retinal pigment epithelial (RPE) cells USMB irradiation was recently found to enhance the uptake rate of two specific endocytic pathways, the clathrin-mediated (CM) and the fluid-phase one [125]. Clathrin-mediated endocytosis requires clathrin protein recruitment at the cell membrane [126] while fluid-phase is a clathrin-independent endocytic mechanism not involving surface receptors or adaptor molecules [127]. The authors evaluated the cell surface expression level of the Transferrin receptor (TfR), a protein which internalises through the CM pathway. Meanwhile, fluid-phase uptake of dextran molecules was monitored through fluorescence measurements. Upon USMB irradiation TfR surface level decreased in less than 5 min as a result of enhanced (CM) endocytosis; instead, more than 10 min where needed to read-out dextran fluorescent uptake increase (fluid-phase endocytic pathway). USMB-mediated enhancement of distinct endocytic pathways could be potentially exploited for improved drug delivery strategies [125].

USMB application also stimulates the complementary process of exocytosis [128] where secretory vesicles export material from intracellular compartments outside cells [122]. USMB-induced molecule release through membrane disruption and enhanced exocytosis is illustrated in [128]. Under intense acoustic pressure (PNP of 570 kPa) specific markers were used to target endosomes — the compartments of the endocytic membrane transport pathway originating from the trans Golgi network — to demonstrate release from different compartments (early/recycling endosomes and lysosomes) in viable cells. Depending on USMB exposure settings, release from the cytoplasm was also observed.

Lysosomes exocytosis occurs upon cell membrane damage [129] and is particularly significant for USMB drug delivery. It is considered among the main membrane repair mechanism upon sonoporation [130] since, during exocytosis, lysosomes fuse with the plasma membrane reconstituting its integrity. Membrane damage leads to increased intracellular calcium level due to diffusion of Ca^{2+} into the cells [117]. In these conditions, a calcium-sensitive protein (synaptotagmin VII) expressed on lysosomal membranes drives enhanced lysosomes exocytosis [130]. Moderate USMB exposure (PNP of 250 kPa) induces transient formation of membrane pores and results into Ca^{2+} entry into the cell thereby stimulating lysosomes exocytosis [130]. Technically, lysosome exocytosis is demonstrated by detecting the relocation of the lysosomal marker protein LAMP-1 at the cell surface. LAMP-1 is normally expressed intracellularly on the lysosomal membrane and undergoes cellular membrane re-

exposure upon membrane damage. LAMP-1 up-regulation at the cell surface of viable cells occurs upon high USMB exposure (PNP 570 kPa), thereby confirming the cellular membrane damage [125].

Low USMB intensity exposure (PNP 100 kPa) determines a variety of intra- and intercellular bio-effects, with negligible impact on cell viability, as shown for HUVEC cells in [113]. Under this US settings, microstreaming also leads to chemical stress and consequent free radicals formation [113], mostly reactive oxygen species (ROS) like H_2O_2 and superoxide. Free radicals increase cell membrane permeability to Ca^{2+}, as demonstrated in cardiomyoblast cells and bovine aortic endothelial cells [113, 124]. A

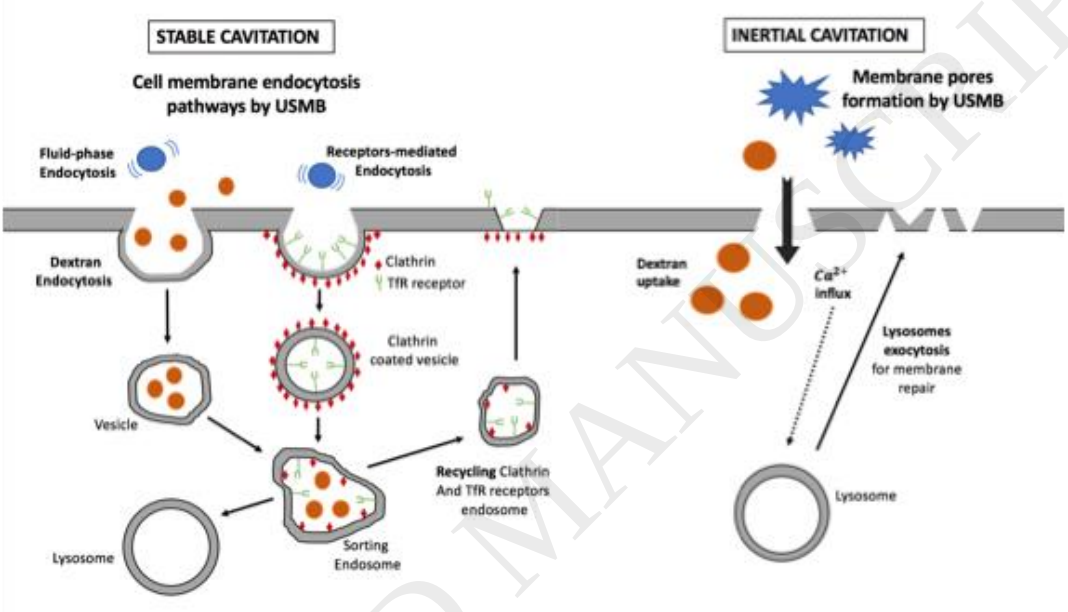

Figure 6. *Schematic representation of USMB-induced endocytosis/exocytosis from cells. Stable cavitation (left side) stimulates cell membrane endocytosis through fluid-phase uptake and receptor-mediated endocytosis. Inertial cavitation (right side) can induce membrane pore formation that leads to Ca^{2+} entry and consequent lysosome exocytosis plus entrance of macromolecules.*

similar phenomenon was observed in Xenopus oocytes and Chinese Hamster Ovary (CHO) cells at a higher PNP (0.3-0.45 MPa) [131, 132]. Other bioeffects of low US exposure concern cytoskeleton rearrangements, as shown in HUVEC by monitoring F-actin re-organisation, one of the main cytoskeleton component, through immunofluorescence [113].

This body of literature confirms that USMB-mediated techniques can be tuned to transiently enhance endothelial barrier permeability, exploiting for controlled delivery concurrent mechanisms of junction loosening, pore formation, endocytosis and exocytosis (see Fig 6).

5. Perspectives of *in vitro* cavitation for drug delivery

Since the 40's FUS (with no bubbles) was tested *in vivo* for noninvasive ablation in the brain and central nervous system lesions [133, 134], but also to alter BBB integrity [135]. The intense ultrasonic irradiation leads, however, to skull heating and beam aberration due to bone irregularities and large acoustic impedance [16]. From the early 2000, microbubbles started to be tested in combination with US in animal models. A brief overview of *in vivo* USMB application is given, prior to deepen into *in vitro* studies.

The typical *in vivo* protocol combines MRI (Magnetic Resonance Imaging) and FUS to stimulate bubble oscillations in a restricted region of interest, with MRI guiding FUS irradiation of the target and monitoring the endothelial response. For BBB opening crucial issues are still the undesired, hardly controlled beam aberration caused by the skull and the scalp.

USMB-mediated drug delivery exploits bubbles to reduce the US threshold for barrier opening. Low intensity FUS were first used after intravenous administration of UCA to induce focal BBB opening *in vivo* in [136]. Sonication was applied on rabbits after craniotomy under MRI guidance and monitoring [136-138]. *In vivo* investigation highlighted that BBB disruption and passage of blood-borne macromolecules (support ed by MRI, light and electron microscopy and histological examination) involve at least four BBB crossing mechanisms: transcythosis, transendothelial opening, i.e. fenestration and channel formation, tight junctions opening and passage through damaged endothelial cells at high US intensity levels [139, 140]. The effect of USMB irradiation on intercellular junction was also investigated. For example, in [141], junction rapture was demonstrated by the loss or reorganisation of immunosignals of tight junctions membrane proteins,(Occludins, Claudin-1 and ZO-1).

BBB opening through intact skin and skull was demonstrated with no need for aberration corrections and minimal beam attenuation and distortion in [142, 143]. This allowed to obtain a significant decrease of the BBB opening pressure threshold with related barrier restoration [144].

I*n vivo* application of USMB-mediated drug delivery was also exploited to test specific drugs extravasation, e.g doxorubicin, a chemotherapeutic agent for the central nervous system [145], and to investigate crucial brain region, e.g. the hippocampus, relevant for neurodegenerative diseases (Alzheimer's) [144, 146-148].

A significant effort aimed at optimising the main USMB protocol parameters, such as ultrasound contrast agents dose, bubble size and sonication parameters, e.g. in [149-152]. Crucial for preventing permanent endothelial damage *in vivo, is* selectively inducing stable vs inertial cavitation using PCD for cavitation detection and quantification. The analysis of UCA emission allowed to understand the role of stable cavitation in the BBB rupture and the not dependence of inertial cavitation threshold on the skull presence, e. g. in [92, 153]. PCD analysis allowed also to demonstrate the correlation existing between cavitation dose, measured by the integral of the cavitation signal power variance, and BBB opening duration, induced permeability and likelihood of negligible damage [154].

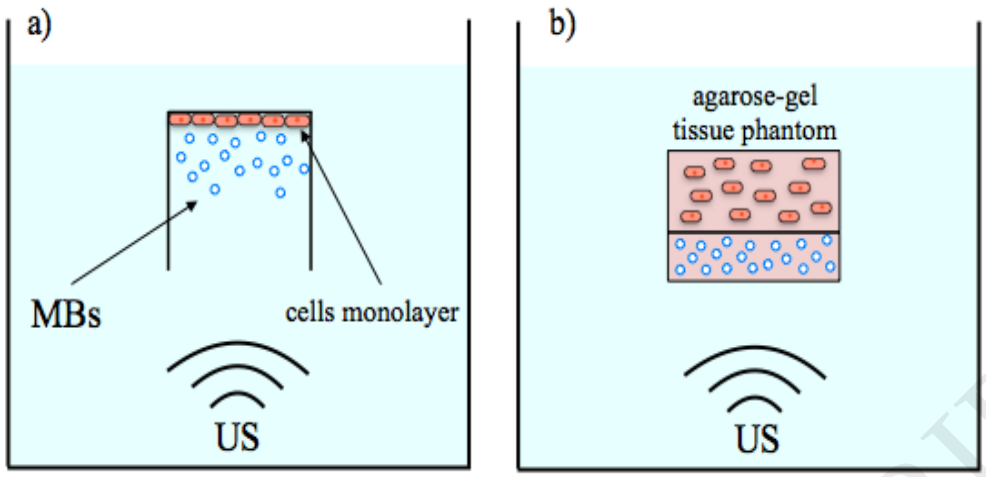

Figure 7. *Schematic of US irradiation of a cell monolayer (a) and an agarose-gel tissue phantom (b).*

The application of USMB in *in vitro* study is considered a valuable alternative to *in vivo* animal models as screening tools for optimising ultrasound mediated drug delivery protocols.

A current *in vitro* model of endothelial barrier consist in a systems comprising a permeable membrane covered with an endothelial monolayer immersed in controlled-temperature liquid tanks (37°C) where USMBs are injected, Fig. 7a.

An example is the cell monolayer grown on an Opticell™ substrate to investigate sonoporation *in vitro* [155] where the interaction of primary pig aortic endothelial cells with US-exposed MBs (Sonovue®) is exhibited. Bubble oscillations induce cell deformation and permeability modification. Deformations are extracted from the displacement of reference points on the cell membrane, while MBs oscillation is measured from the instantaneous diameter. The fast 1 MHz oscillations are observed with a the Bandaris 128 camera [156]. This camera is capable of acquiring a sequence of 128 consecutive image frames with 500 x 292 pixels at a maximum rate of 25 million frame/s.

The feasibility of controlled cavitation-induced increase of HUVEC endothelial monolayer permeability is investigate with a similar set-up in [157]. Prior and upon US exposure, the permeability is determined from transendothelial electrical resistance (TEER) data. TEER is sensitive to endothelial layer integrity changes, membrane permeability alterations and tight junction formation [158]. USMBs are found to significantly reduce TEER, i.e. increase permeability, with no impact on cell viability [157].

Recently, a BBB model of primary porcine brain endothelial cells (PBECs) was investigated under stable and inertial cavitation in [159]. A tight PBEC monolayer was grown on a permeable membrane and was immersed upside down in phosphate buffered solution (PBS) in a sonicator containing SonoVue® MBs to acquire the backscattered signal by PCD. Possible limitations of the approach due to the high

sensitivity and fragility of PBEC monolayers were highlighted by the authors. Absence of flow component is also worth noticing.

Tissue phantom models are alternative to cells monolayer-based systems (see Fig 7b). They consist of an agarose-gel tissue platform optimised to hold the bubble suspension and are ideal to study tissue-like response to USMB irradiation. Cavitation activity and acoustic parameters needed to obtain desired bioeffects were checked by such devices in a recent paper [107].
Tissue-mimicking phantoms under flow were already exploited to assess USMB-induced macromolecule extravasation from a vessel-gel-system [160]. The gel encased with breast cancer cells was irradiated with US to evaluate extravasation with/without MBs assistance and to assess cell viability. Data are obtained by means of PCD and phase-contrast imaging.

Microvessels-on-a-chip have been used for US-assisted drug delivery in [161]. The microfluidic chip mimics *in vivo* microvascular beds with stable cavitation stimulating receptor-mediated endocytosis. The network consists of a central and two side, parallel cell-cultured channels separated from the central one by two additional fluidic channels [162]. Medium exchange across channels is ensured by microposts. Channels are seeded with fibroblasts and HUVECs while functionalized MBs are diluted in the medium and loaded in the microdevice reservoirs. US exposure is provided by a single-element, spherically focused transducer (1.1 MHz) while PCD acquires the bubble acoustic signature (5 MHz). The work demonstrates the potential of such devices to optimise USMB-mediated drug delivery in cheap and easy-to-handle set-ups. The main limitation is the absence of flow and related shear stress.

The *in vitro* devices discussed so far represent a significant progress in the development of USMB mediated drug delivery systems alternative/complementary to *in vivo* animal experimentation. From the bibliography a high fidelity fluid flow component able to reproduce the physiological conditions emerges as a crucial missing feature in view of developing reliable endothelial barrier models. Under this respect, microfluidic platforms which combine the USMB-mediated approach with vasculature networks under proper flow conditions could greatly facilitate the assessment of strategies for barrier permeability enhancement.

The conditions encountered in the application of USMB-mediated drug delivery in animal models involve a typical microvasculature lumen in the range of $40 - 110\mu$m and typical shear stress on vessel walls of the order of 10^{-2} dyne/cm^2, corresponding to a flow rate of 0.2 μl/min [57, 163].
The stationary flow in the capillaries is accurately reproduced by standard syringe pumps. Moreover, available soft lithography techniques allow to produce both elementary microvessels and the complex network of an actual capillary bed [53]. Intravital microscopy was already used to acquire and digitise images of capillary networks to be reproduced by microfabrication [164]. Suitably designed tissue

chambers can be integrated with vasculature models of various complexity to host different target tissues, either healthy or diseased, communicating with the vessels through the endothelial barrier. Where needed, a microbubble generator can be added to enable control of MBs characteristics (e.g. monodispersity, kind of shell, shell integrity and functionalisation).

Protocols for growing endothelia in the artificial vessels are already well developed. The exposition of the cells to physiological shear stresses is crucial to strengthen the endothelial phenotype allowing the cells to assume the characteristic shape elongated in the streamwise direction. Cells density standardisation is also important to obtain the proper physiological/pathological endothelial cell coverage, see Fig. 1. After MBs injection in the artificial vasculature, the biomimetic device can be irradiated with US adopting different protocols. Cavitation activity can be monitored through, e.g., PCD, while permeability measurement can be obtained through fluorescence imaging or radioisotope tagging. Staining with specific markers can be used to evaluate cell viability, cell-cell interaction changes (junction rupture), cytoskeleton reorganisation and membrane integrity restoration.

In conclusion, the potential of *in vitro* platforms for targeted drug delivery in general, and USMB-assisted extravasation in particular, is substantial. Such microfluidic devices offer a number of advantages when used in parallel/in alternative to more traditional *in vivo* approaches. The stability and reproducibility of artificial blood vessels mimicking the relevant physiological and pathological microenvironment allow a precise assessment of cavitation effects on the endothelial barrier and may help developing optimised protocols to minimise endothelial damage. *In vitro* approaches are expected to significantly reduce costs and time of pharmaceutical trials by offering cheap and reliable information for prescreening before resorting to a limited number of precisely aimed *in vivo* experiments. Not to mention ethical issues, reducing animal experimentation and resorting to related animal facilities have big impact on clinical and pharmaceutical research not only in terms of direct economic savings but also in terms of laboratory simplification. Cost and complexity of health care systems are in fact a central issue in modern countries. Given the European healthcare budget running around 800 billion euro per year for the sole central nervous system disorders [165] and the progressive ageing of the population, reduction of developing time for reliable and cost-effective drug delivery procedures is indeed a social priority.

Acknowledgements

This work was supported by the European Research Council under the ERC-2017-PoC Grant Agreement no. 779751. We would like to thank Prof. M.F. Kiani for the invaluable discussions and insights provided on the BBB-on-a-chip biological functionalisation. For the original results we acknowledge our collaborators: F. Alves Pereira, D. Caprini, M. Chinappi, L. Marino and C. Scognamiglio.

Bibliography

1. Torchilin, V.P., *Drug targeting.* European Journal of Pharmaceutical Sciences, 2000. **11**: p. S81-S91.
2. Bae, Y.H. and K. Park, Targeted drug delivery to tumors: myths, reality and possibility. Journal of Controlled Release, 2011. **153**(3): p. 198.
3. Hoffman, A.S., The origins and evolution of "controlled" drug delivery systems. Journal of Controlled Release, 2008. **132**(3): p. 153-163.
4. Strebhardt, K. and A. Ullrich, Paul Ehrlich's magic bullet concept: 100 years of progress. Nature Reviews Cancer, 2008. **8**(6): p. 473-480.
5. Mills, J.K. and D. Needham, *Targeted drug delivery.* Expert Opinion on Therapeutic Patents, 1999. **9**(11): p. 1499-1513.
6. Minchinton, A.I. and I.F. Tannock, *Drug penetration in solid tumours.* Nature reviews. Cancer, 2006. **6**(8): p. 583.
7. Langer, R., Drug deliveryand targeting. Nature, 1998. **392**(6679): p. 5-10.
8. Khan, I.U., et al., Microfluidics: a focus on improved cancer targeted drug delivery systems. Journal of controlled release, 2013. **172**(3): p. 1065-1074.
9. Whitesides, G.M., The origins and the future of microfluidics. Nature, 2006. **442**(7101): p. 368.
10. Wang, T.-Y., et al., Ultrasound and microbubble guided drug delivery: mechanistic understanding and clinical implications. Current pharmaceutical biotechnology, 2014. **14**(8): p. 743-752.
11. Unger, E., et al., Cardiovascular drug delivery with ultrasound and microbubbles. Advanced drug delivery reviews, 2014. **72**: p. 110-126.
12. Gramiak, R. and P.M. Shah, Echocardiography of the aortic root. Investigative radiology, 1968. **3**(5): p. 356-366.
13. Lindner, J.R., Microbubbles in medical imaging: current applications and future directions. Nature Reviews Drug Discovery, 2004. **3**(6): p. 527-533.
14. Cosgrove, D., Ultrasound contrast agents: an overview. European journal of radiology, 2006. **60**(3): p. 324-330.
15. Konofagou, E.E., Optimization of the ultrasound-induced blood-brain barrier opening. Theranostics, 2012. **2**(12): p. 1223.
16. Aryal, M., et al., Ultrasound-mediated blood–brain barrier disruption for targeted drug delivery in the central nervous system. Advanced drug delivery reviews, 2014. **72**: p. 94-109.
17. Kooiman, K., et al., Acoustic behavior of microbubbles and implications for drug delivery. Advanced drug delivery reviews, 2014. **72**: p. 28-48.
18. Negishi, Y., Y. Endo-Takahashi, and K. Maruyama, Gene delivery systems by the combination of lipid bubbles and ultrasound. Drug discoveries & therapeutics, 2016. **10**(5): p. 248-255.
19. Brennen, C.E., *Cavitation in medicine.* Interface focus, 2015. **5**(5): p. 20150022.
20. Liu, H.-L., et al., Combining microbubbles and ultrasound for drug delivery to brain tumors: current progress and overview. Theranostics, 2014. **4**(4): p. 432.
21. Pardridge, W.M., The blood-brain barrier: bottleneck in brain drug development. NeuroRx, 2005. **2**(1): p. 3-14.
22. Rondeau, E. and J.J. Cooper-White, Biopolymer microparticle and nanoparticle formation within a microfluidic device. Langmuir, 2008. **24**(13): p. 6937-6945.
23. Hung, L.-H., et al., PLGA micro/nanosphere synthesis by droplet microfluidic solvent evaporation and extraction approaches. Lab on a Chip, 2010. **10**(14): p. 1820-1825.

24. Serra, C.A., et al., *Microfluidic Production of Micro-and Nanoparticles.* Encyclopedia of Polymer Science and Technology, 2013.
25. Liu, L. and S. Choi, Self-Sustainable, High-Power-Density Bio-Solar Cells for Lab-on-a-Chip Applications. Lab on a Chip, 2017.
26. Lavan, D.A., T. McGuire, and R. Langer, Small-scale systems for in vivo drug delivery. Nature biotechnology, 2003. **21**(10): p. 1184.
27. Riahi, R., et al., Microfluidics for advanced drug delivery systems. Current Opinion in Chemical Engineering, 2015. **7**: p. 101-112.
28. Kim, S., et al., Vasculature-on-a-chip for in vitro disease models. Bioengineering, 2017. **4**(1): p. 8.
29. Parlato, S., et al., 3D Microfluidic model for evaluating immunotherapy efficacy by tracking dendritic cell behaviour toward tumor cells. Scientific Reports, 2017. **7**.
30. Sackmann, E.K., A.L. Fulton, and D.J. Beebe, The present and future role of microfluidics in biomedical research. Nature, 2014. **507**(7491): p. 181.
31. Esch, E.W., A. Bahinski, and D. Huh, Organs-on-chips at the frontiers of drug discovery. Nature reviews. Drug discovery, 2015. **14**(4): p. 248.
32. Anderson, J.R., et al., Fabrication of topologically complex three-dimensional microfluidic systems in PDMS by rapid prototyping. Analytical chemistry, 2000. **72**(14): p. 3158-3164.
33. Anderson, J.R., et al., Fabrication of microfluidic systems in poly (dimethylsiloxane). Electrophoresis, 2000. **21**(1): p. 27-40.
34. Sia, S.K. and G.M. Whitesides, Microfluidic devices fabricated in poly (dimethylsiloxane) for biological studies. Electrophoresis, 2003. **24**(21): p. 3563-3576.
35. Toepke, M.W. and D.J. Beebe, PDMS absorption of small molecules and consequences in microfluidic applications. Lab on a Chip, 2006. **6**(12): p. 1484-1486.
36. Lorenz, H., et al., *SU-8: a low-cost negative resist for MEMS.* Journal of Micromechanics and Microengineering, 1997. **7**(3): p. 121.
37. Caprini, D., et al. Rapid prototyping of glass microfluidic chips based on autonomous capillary networks for physiological solutions. in AISEM Annual Conference, 2015 XVIII. 2015. IEEE.
38. Xia, Y. and G.M. Whitesides, *Soft lithography.* Annual review of materials science, 1998. **28**(1): p. 153-184.
39. Cucullo, L., et al., A new dynamic in vitro model for the multidimensional study of astrocyte–endothelial cell interactions at the blood–brain barrier. Brain research, 2002. **951**(2): p. 243-254.
40. Cucullo, L., et al., Immortalized human brain endothelial cells and flow-based vascular modeling: a marriage of convenience for rational neurovascular studies. Journal of Cerebral Blood Flow & Metabolism, 2008. **28**(2): p. 312-328.
41. Nakagawa, S., et al., A new blood–brain barrier model using primary rat brain endothelial cells, pericytes and astrocytes. Neurochemistry international, 2009. **54**(3): p. 253-263.
42. Prabhakarpandian, B., et al., SyM-BBB: a microfluidic blood brain barrier model. Lab on a chip, 2013. **13**(6): p. 1093-1101.
43. Wang, J.D., et al., Organization of endothelial cells, pericytes, and astrocytes into a 3D microfluidic in vitro model of the blood–brain Barrier. Molecular pharmaceutics, 2016. **13**(3): p. 895-906.
44. Helms, H.C., et al., In vitro models of the blood–brain barrier: an overview of commonly used brain endothelial cell culture models and guidelines for their use. Journal of Cerebral Blood Flow & Metabolism, 2016. **36**(5): p. 862-890.

45. Phan, D.T., et al., Blood–brain barrier-on-a-chip: Microphysiological systems that capture the complexity of the blood–central nervous system interface. Experimental Biology and Medicine, 2017: p. 1535370217694100.
46. Resnick, N., et al., Fluid shear stress and the vascular endothelium: for better and for worse. Progress in biophysics and molecular biology, 2003. **81**(3): p. 177-199.
47. Tzima, E., et al., A mechanosensory complex that mediates the endothelial cell response to fluid shear stress. Nature, 2005. **437**(7057): p. 426.
48. DuFort, C.C., M.J. Paszek, and V.M. Weaver, Balancing forces: architectural control of mechanotransduction. Nature reviews. Molecular cell biology, 2011. **12**(5): p. 308.
49. Cucullo, L., et al., The role of shear stress in Blood-Brain Barrier endothelial physiology. BMC neuroscience, 2011. **12**(1): p. 40.
50. Song, J.W. and L.L. Munn, *Fluid forces control endothelial sprouting.* Proceedings of the National Academy of Sciences, 2011. **108**(37): p. 15342-15347.
51. Brown, D.C. and R.S. Larson, Improvements to parallel plate flow chambers to reduce reagent and cellular requirements. BMC immunology, 2001. **2**(1): p. 9.
52. Prabhakarpandian, B., et al., Synthetic microvascular networks for quantitative analysis of particle adhesion. Biomedical microdevices, 2008. **10**(4): p. 585-595.
53. Lamberti, G., et al., Bioinspired microfluidic assay for in vitro modeling of leukocyte–endothelium interactions. Analytical chemistry, 2014. **86**(16): p. 8344-8351.
54. Cucullo, L., et al., A dynamic in vitro BBB model for the study of immune cell trafficking into the central nervous system. Journal of Cerebral Blood Flow & Metabolism, 2011. **31**(2): p. 767-777.
55. Booth, R. and H. Kim, Characterization of a microfluidic in vitro model of the blood-brain barrier (μBBB). Lab on a chip, 2012. **12**(10): p. 1784-1792.
56. Herland, A., et al., Distinct contributions of astrocytes and pericytes to neuroinflammation identified in a 3D human blood-brain barrier on a chip. PLoS One, 2016. **11**(3): p. e0150360.
57. Deosarkar, S.P., et al., A novel dynamic neonatal blood-brain barrier on a chip. PloS one, 2015. **10**(11): p. e0142725.
58. Terrell-Hall, T.B., et al., Permeability across a novel microfluidic blood-tumor barrier model. Fluids and Barriers of the CNS, 2017. **14**(1): p. 3.
59. De Luca, R., et al. Towards cavitation-enhanced permeability in blood vessel on a chip. in AIP Conference Proceedings. 2017. AIP Publishing.
60. Boissenot, T., et al., Ultrasound-triggered drug delivery for cancer treatment using drug delivery systems: From theoretical considerations to practical applications. Journal of Controlled Release, 2016. **241**: p. 144-163.
61. Apfel, R.E. and C.K. Holland, Gauging the likelihood of cavitation from short-pulse, low-duty cycle diagnostic ultrasound. Ultrasound in medicine & biology, 1991. **17**(2): p. 179-185.
62. Barnett, S.B., et al., International recommendations and guidelines for the safe use of diagnostic ultrasound in medicine. Ultrasound in medicine & biology, 2000. **26**(3): p. 355-366.
63. Brennen, C.E., *Cavitation and bubble dynamics*. 2013: Cambridge University Press.
64. Rayleigh, L., *VIII. On the pressure developed in a liquid during the collapse of a spherical cavity.* The London, Edinburgh, and Dublin Philosophical Magazine and Journal of Science, 1917. **34**(200): p. 94-98.
65. Plesset, M.S., *The dynamics of cavitation bubbles.* Journal of applied mechanics, 1949. **16**: p. 277-282.

66. Blake Jr, F.G., *Onset of Cavitation in Liquids: I,* in *Acoustic Research Laboratory,* T.M. No.12, Editor. 1949, Harvard University.
67. Apfel, R., *Possibility of microcavitation from diagnostic ultrasound.* IEEE transactions on ultrasonics, ferroelectrics, and frequency control, 1986. **33**(2): p. 139-142.
68. Holland, C.K. and R.E. Apfel, *An improved theory for the prediction of microcavitation thresholds.* IEEE transactions on ultrasonics, ferroelectrics, and frequency control, 1989. **36**(2): p. 204-208.
69. Vogel, A., S. Busch, and U. Parlitz, Shock wave emission and cavitation bubble generation by picosecond and nanosecond optical breakdown in water. The Journal of the Acoustical Society of America, 1996. **100**(1): p. 148-165.
70. Ohl, C.D., et al., *Bubble dynamics, shock waves and sonoluminescence.* Philosophical Transactions of the Royal Society of London A: Mathematical, Physical and Engineering Sciences, 1999. **357**(1751): p. 269-294.
71. Lauterborn, W. and A. Vogel, *Shock wave emission by laser generated bubbles.* Bubble dynamics and shock waves, 2013: p. 67-103.
72. Magaletti, F., L. Marino, and C.M. Casciola, Shock wave formation in the collapse of a vapor nanobubble. Physical review letters, 2015. **114**(6): p. 064501.
73. Epstein, P. and M.S. Plesset, On the stability of gas bubbles in liquid-gas solutions. The Journal of Chemical Physics, 1950. **18**(11): p. 1505-1509.
74. Duncan, P.B. and D. Needham, Test of the Epstein− Plesset Model for Gas Microparticle Dissolution in Aqueous Media: Effect of Surface Tension and Gas Undersaturation in Solution. Langmuir, 2004. **20**(7): p. 2567-2578.
75. Kwan, J.J. and M.A. Borden, Lipid monolayer collapse and microbubble stability. Advances in colloid and interface science, 2012. **183**: p. 82-99.
76. Wu, J. and W.L. Nyborg, Ultrasound, cavitation bubbles and their interaction with cells. Advanced drug delivery reviews, 2008. **60**(10): p. 1103-1116.
77. Guo, X., et al., Investigation on the inertial cavitation threshold and shell properties of commercialized ultrasound contrast agent microbubbles. The Journal of the Acoustical Society of America, 2013. **134**(2): p. 1622-1631.
78. Sirsi, S.R. and M.A. Borden, State-of-the-art materials for ultrasound-triggered drug delivery. Advanced drug delivery reviews, 2014. **72**: p. 3-14.
79. de Jong, N., et al., Absorption and scatter of encapsulated gas filled microspheres: theoretical considerations and some measurements. Ultrasonics, 1992. **30**(2): p. 95-103.
80. Church, C.C., The effects of an elastic solid surface layer on the radial pulsations of gas bubbles. The Journal of the Acoustical Society of America, 1995. **97**(3): p. 1510-1521.
81. Hoff, L., P.C. Sontum, and J.M. Hovem, Oscillations of polymeric microbubbles: Effect of the encapsulating shell. The Journal of the Acoustical Society of America, 2000. **107**(4): p. 2272-2280.
82. Marmottant, P., et al., A model for large amplitude oscillations of coated bubbles accounting for buckling and rupture. The Journal of the Acoustical Society of America, 2005. **118**(6): p. 3499-3505.
83. De Jong, N., et al., "Compression-only" behavior of phospholipid-coated contrast bubbles. Ultrasound in medicine & biology, 2007. **33**(4): p. 653-656.
84. Frinking, P.J. and N. de Jong, Acoustic modeling of shell-encapsulated gas bubbles. Ultrasound in medicine & biology, 1998. **24**(4): p. 523-533.
85. Chowdhury, S.M., T. Lee, and J.K. Willmann, *Ultrasound-guided drug delivery in cancer.* Ultrasonography, 2017. **36**(3): p. 171.

86. Kolb, J. and W.L. Nyborg, *Small-scale acoustic streaming in liquids.* The Journal of the Acoustical Society of America, 1956. **28**(6): p. 1237-1242.
87. Lighthill, J., *Acoustic streaming.* Journal of sound and vibration, 1978. **61**(3): p. 391-418.
88. Nyborg, W.L., *Acoutic Streaming. In Nonlinear acoustics*. Vol. 1. 1998: Academic press San Diego.
89. Tho, P., R. Manasseh, and A. Ooi, Cavitation microstreaming patterns in single and multiple bubble systems. Journal of fluid mechanics, 2007. **576**: p. 191-233.
90. Batchelor, G.K., *An introduction to fluid dynamics*. 2000: Cambridge university press.
91. Longuet-Higgins, M.S. Viscous streaming from an oscillating spherical bubble. in Proceedings of the Royal Society of London A: Mathematical, Physical and Engineering Sciences. 1998. The Royal Society.
92. Tung, Y.-S., et al., In vivo transcranial cavitation threshold detection during ultrasound-induced blood–brain barrier opening in mice. Physics in medicine and biology, 2010. **55**(20): p. 6141.
93. Dalecki, D., Mechanical bioeffects of ultrasound. Annu. Rev. Biomed. Eng., 2004. **6**: p. 229-248.
94. Plesset, M.S. and R.B. Chapman, Collapse of an initially spherical vapour cavity in the neighbourhood of a solid boundary. Journal of Fluid Mechanics, 1971. **47**(2): p. 283-290.
95. Lauterborn, W. and H. Bolle, Experimental investigations of cavitation-bubble collapse in the neighbourhood of a solid boundary. Journal of Fluid Mechanics, 1975. **72**(2): p. 391-399.
96. Herring, C., Theory of the pulsations of the gas bubble produced by an underwater explosion, in US Nat. Defence Res. Comm. Report. 1941.
97. Davies, R. and G. Taylor, The vertical motion of a spherical bubble and the pressure surrounding it. The Scientific Papers of GI Taylor, 1942: p. 320-336.
98. Davies, R. and G. Taylor, The motion and shape of the hollow produced by an explosion in a liquid. The Scientific Papers of GI Taylor, 1943: p. 337-353.
99. Vogel, A., W. Lauterborn, and R. Timm, Optical and acoustic investigations of the dynamics of laser-produced cavitation bubbles near a solid boundary. Journal of Fluid Mechanics, 1989. **206**: p. 299-338.
100. Philipp, A. and W. Lauterborn, Cavitation erosion by single laser-produced bubbles. Journal of Fluid Mechanics, 1998. **361**: p. 75-116.
101. Ohl, C.-D., et al., Surface cleaning from laser-induced cavitation bubbles. Applied physics letters, 2006. **89**(7): p. 074102.
102. Birkhoff, G., *Hydrodynamics*. 2015: Princeton University Press.
103. Blake, J., Y. Tomita, and R. Tong, The art, craft and science of modelling jet impact in a collapsing cavitation bubble, in In Fascination of Fluid Dynamics. 1998, Springer. p. 77-90.
104. Magaletti, F., et al., The sharp-interface limit of the Cahn–Hilliard/Navier–Stokes model for binary fluids. Journal of Fluid Mechanics, 2013. **714**: p. 95-126.
105. Magaletti, F., et al., Shock-induced collapse of a vapor nanobubble near solid boundaries. International Journal of Multiphase Flow, 2016. **84**: p. 34-45.
106. Wan, M., Y. Feng, and G. ter Haar, *Cavitation in Biomedicine*. 2015: Springer.
107. Lin, Y., et al., Effect of acoustic parameters on the cavitation behavior of SonoVue microbubbles induced by pulsed ultrasound. Ultrasonics sonochemistry, 2017. **35**: p. 176-184.

108. Komarova, Y. and A.B. Malik, Regulation of endothelial permeability via paracellular and transcellular transport pathways. Annual review of physiology, 2010. **72**: p. 463-493.
109. Tsukita, S., M. Furuse, and M. Itoh, *Multifunctional strands in tight junctions.* Nature reviews Molecular cell biology, 2001. **2**(4): p. 285-293.
110. Carmeliet, P., et al., Targeted deficiency or cytosolic truncation of the VE-cadherin gene in mice impairs VEGF-mediated endothelial survival and angiogenesis. Cell, 1999. **98**(2): p. 147-157.
111. Crosby, C.V., et al., VE-cadherin is not required for the formation of nascent blood vessels but acts to prevent their disassembly. Blood, 2005. **105**(7): p. 2771-2776.
112. Huber, A.H., et al., The Cadherin Cytoplasmic Domain Is Unstructured in the Absence of β-Catenin A POSSIBLE MECHANISM FOR REGULATING CADHERIN TURNOVER. Journal of Biological Chemistry, 2001. **276**(15): p. 12301-12309.
113. Juffermans, L.J., et al., Ultrasound and microbubble-induced intra-and intercellular bioeffects in primary endothelial cells. Ultrasound in medicine & biology, 2009. **35**(11): p. 1917-1927.
114. Miller, D.L., S. Bao, and J.E. Morris, Sonoporation of cultured cells in the rotating tube exposure system. Ultrasound in medicine & biology, 1999. **25**(1): p. 143-149.
115. Ward, M., J. Wu, and J.-F. Chiu, Ultrasound-induced cell lysis and sonoporation enhanced by contrast agents. The Journal of the Acoustical Society of America, 1999. **105**(5): p. 2951-2957.
116. Ross, J.P., et al., Optical and atomic force microscopic studies on sonoporation. The Journal of the Acoustical Society of America, 2002. **111**(3): p. 1161-1164.
117. Juffermans, L., et al., Transient permeabilization of cell membranes by ultrasound-exposed microbubbles is related to formation of hydrogen peroxide. American Journal of Physiology-Heart and Circulatory Physiology, 2006. **291**(4): p. H1595-H1601.
118. Schlicher, R.K., et al., Mechanism of intracellular delivery by acoustic cavitation. Ultrasound in medicine & biology, 2006. **32**(6): p. 915-924.
119. De Cock, I., et al., Ultrasound and microbubble mediated drug delivery: acoustic pressure as determinant for uptake via membrane pores or endocytosis. Journal of controlled release, 2015. **197**: p. 20-28.
120. Tachibana, K., et al., Induction of cell-membrane porosity by ultrasound. The Lancet, 1999. **353**(9162): p. 1409.
121. Mehier-Humbert, S., et al., Plasma membrane poration induced by ultrasound exposure: implication for drug delivery. Journal of controlled release, 2005. **104**(1): p. 213-222.
122. Gundelfinger, E.D., M.M. Kessels, and B. Qualmann, Temporal and spatial coordination of exocytosis and endocytosis. Nature reviews molecular cell biology, 2003. **4**(2): p. 127-139.
123. Peruzzi, G., et al., Endocytosis as a mechanism of regulating natural killer cell function: unique endocytic and trafficking pathway for CD94/NKG2A. Immunologic research, 2009. **43**(1-3): p. 210-222.
124. Meijering, B.D., et al., Ultrasound and microbubble-targeted delivery of macromolecules is regulated by induction of endocytosis and pore formation. Circulation research, 2009. **104**(5): p. 679-687.

125. Fekri, F., et al., Ultrasound Microbubble Treatment Enhances Clathrin-Mediated Endocytosis and Fluid-Phase Uptake through Distinct Mechanisms. PloS one, 2016. **11**(6): p. e0156754.
126. Conner, S.D. and S.L. Schmid, Regulated portals of entry into the cell. Nature, 2003. **422**(6927): p. 37-44.
127. Mayor, S. and R.E. Pagano, *Pathways of clathrin-independent endocytosis.* Nature reviews Molecular cell biology, 2007. **8**(8): p. 603-612.
128. Hussein, F., C. Antonescu, and R. Karshafian, Ultrasound and microbubble induced release from intracellular compartments. BMC biotechnology, 2017. **17**(1): p. 45.
129. Reddy, A., E.V. Caler, and N.W. Andrews, Plasma membrane repair is mediated by Ca 2+-regulated exocytosis of lysosomes. Cell, 2001. **106**(2): p. 157-169.
130. Yang, F., et al., Experimental study on cell self-sealing during sonoporation. Journal of Controlled Release, 2008. **131**(3): p. 205-210.
131. Pan, H., et al., Study of sonoporation dynamics affected by ultrasound duty cycle. Ultrasound in medicine & biology, 2005. **31**(6): p. 849-856.
132. Kumon, R.E., et al., Ultrasound-induced calcium oscillations and waves in Chinese hamster ovary cells in the presence of microbubbles. Biophysical journal, 2007. **93**(6): p. L29-L31.
133. Fry, W.J., et al., Production of focal destructive lesions in the central nervous system with ultrasound. Journal of neurosurgery, 1954. **11**(5): p. 471-478.
134. Ballantine Jr, H., E. Bell, and J. Manlapaz, Progress and problems in the neurological applications of focused ultrasound. Journal of neurosurgery, 1960. **17**(5): p. 858-876.
135. Bakay, L., et al., Ultrasonically produced changes in the blood-brain barrier. AMA Archives of Neurology & Psychiatry, 1956. **76**(5): p. 457-467.
136. Hynynen, K., et al., Noninvasive MR imaging–guided focal opening of the blood-brain barrier in rabbits. Radiology, 2001. **220**(3): p. 640-646.
137. Hynynen, K., et al., A clinical, noninvasive, MR imaging-monitored ultrasound surgery method. Radiographics, 1996. **16**(1): p. 185-195.
138. Hynynen, K., et al., Local and reversible blood–brain barrier disruption by noninvasive focused ultrasound at frequencies suitable for trans-skull sonications. Neuroimage, 2005. **24**(1): p. 12-20.
139. Sheikov, N., et al., Cellular mechanisms of the blood-brain barrier opening induced by ultrasound in presence of microbubbles. Ultrasound in medicine & biology, 2004. **30**(7): p. 979-989.
140. Sheikov, N., et al., Brain arterioles show more active vesicular transport of blood-borne tracer molecules than capillaries and venules after focused ultrasound-evoked opening of the blood-brain barrier. Ultrasound in medicine & biology, 2006. **32**(9): p. 1399-1409.
141. Sheikov, N., et al., Effect of focused ultrasound applied with an ultrasound contrast agent on the tight junctional integrity of the brain microvascular endothelium. Ultrasound in medicine & biology, 2008. **34**(7): p. 1093-1104.
142. Choi, J.J., et al. Feasibility of transcranial, localized drug-delivery in the brain of Alzheimer's-model mice using focused ultrasound. in Ultrasonics Symposium, 2005 IEEE. 2005. IEEE.
143. Choi, J.J., et al., Noninvasive, transcranial and localized opening of the blood-brain barrier using focused ultrasound in mice. Ultrasound in medicine & biology, 2007. **33**(1): p. 95-104.

144. Choi, J., et al., Spatio-temporal analysis of molecular delivery through the blood–brain barrier using focused ultrasound. Physics in medicine and biology, 2007. **52**(18): p. 5509.
145. Treat, L.H., et al., Targeted delivery of doxorubicin to the rat brain at therapeutic levels using MRI-guided focused ultrasound. International journal of cancer, 2007. **121**(4): p. 901-907.
146. Choi, J.J., et al., Noninvasive and transient blood-brain barrier opening in the hippocampus of Alzheimer's double transgenic mice using focused ultrasound. Ultrasonic imaging, 2008. **30**(3): p. 189-200.
147. Konofagou, E. and J. Choi, Ultrasound-induced treatment of neurodegenerative diseases across the blood-brain barrier, in Biomedical Applications of Vibration and Acoustics in Therapy, Bioeffect and Modeling. 2008, ASME Press.
148. Choi, J.J., et al., Molecules of various pharmacologically-relevant sizes can cross the ultrasound-induced blood-brain barrier opening in vivo. Ultrasound in medicine & biology, 2010. **36**(1): p. 58-67.
149. Yang, F.-Y., et al., Quantitative evaluation of focused ultrasound with a contrast agent on blood-brain barrier disruption. Ultrasound in medicine & biology, 2007. **33**(9): p. 1421-1427.
150. Baseri, B., et al., Multi-modality safety assessment of blood-brain barrier opening using focused ultrasound and definity microbubbles: a short-term study. Ultrasound in medicine & biology, 2010. **36**(9): p. 1445-1459.
151. Tung, Y.-S., et al., The mechanism of interaction between focused ultrasound and microbubbles in blood-brain barrier opening in mice. The Journal of the Acoustical Society of America, 2011. **130**(5): p. 3059-3067.
152. McDannold, N., et al., Temporary disruption of the blood–brain barrier by use of ultrasound and microbubbles: safety and efficacy evaluation in rhesus macaques. Cancer research, 2012. **72**(14): p. 3652-3663.
153. McDannold, N., N. Vykhodtseva, and K. Hynynen, Targeted disruption of the blood–brain barrier with focused ultrasound: association with cavitation activity. Physics in medicine and biology, 2006. **51**(4): p. 793.
154. Sun, T., et al., Acoustic cavitation-based monitoring of the reversibility and permeability of ultrasound-induced blood-brain barrier opening. Physics in medicine and biology, 2015. **60**(23): p. 9079.
155. van Wamel, A., et al., Micromanipulation of endothelial cells: ultrasound-microbubble-cell interaction. Ultrasound in medicine & biology, 2004. **30**(9): p. 1255-1258.
156. Chin, C.T., et al., Brandaris 128: A digital 25 million frames per second camera with 128 highly sensitive frames. Review of scientific instruments, 2003. **74**(12): p. 5026-5034.
157. Kooiman, K., et al., Increasing the endothelial layer permeability through ultrasound-activated microbubbles. IEEE Transactions on Biomedical Engineering, 2010. **57**(1): p. 29-32.
158. Gautam, N., P. Hedqvist, and L. Lindbom, Kinetics of leukocyte-induced changes in endothelial barrier function. British journal of pharmacology, 1998. **125**(5): p. 1109-1114.
159. Lélu, S., et al., Primary Porcine Brain Endothelial Cells as In Vitro Model to Study Effects of Ultrasound and Microbubbles on Blood–Brain Barrier Function. IEEE transactions on ultrasonics, ferroelectrics, and frequency control, 2017. **64**(1): p. 281-290.

160. Arvanitis, C.D., et al., Cavitation-enhanced extravasation for drug delivery. Ultrasound in medicine & biology, 2011. **37**(11): p. 1838-1852.
161. Park, Y.C., et al., Microvessels-on-a-Chip to Assess Targeted Ultrasound-Assisted Drug Delivery. ACS applied materials & interfaces, 2016. **8**(46): p. 31541-31549.
162. Kim, S., et al., Engineering of functional, perfusable 3D microvascular networks on a chip. Lab on a Chip, 2013. **13**(8): p. 1489-1500.
163. Fung, Y.-c., *Biomechanics: circulation*. 2013: Springer Science & Business Media.
164. Rosano, J.M., et al., A physiologically realistic in vitro model of microvascular networks. Biomedical microdevices, 2009. **11**(5): p. 1051.
165. Gustavsson, A., et al., Cost of disorders of the brain in Europe 2010. European neuropsychopharmacology, 2011. **21**(10): p. 718-779.